Energy Proceedings
Vol 54, 2025
ISSN 2004-2965

Internal Microstructural Changes and Side Reactions Induced by Copper Impurity Particles in Lithium-Ion Batteries#

Shun Chen[1], Jufeng Yang[1,2], Guodong Fan[1], Siyi Ye[1], Bangjun Guo[1], Yansong Wang[1], Xi Zhang[1*]

1 School of Mechanical Engineering, Shanghai Jiao Tong University, 800 Dongchuan Road, Shanghai, 200240, China

2 Automotive Engineering Research Institute, Jiangsu University, 301 Xuefu Road, Zhenjiang, Jiangsu 212013, China

(Corresponding Author: braver1980@sjtu.edu.cn)

ABSTRACT

Lithium-ion batteries serve as crucial energy storage carriers due to their numerous superior properties. However, metal impurities introduced during the manufacturing process can affect battery performance. The intrinsic impacts of these impurities have not yet been fully elucidated. In this study, pouch cells containing copper particle impurities are investigated. The results show that cells with impurities not only experienced micro-short circuits but also exhibited higher polarization compared to normal cells. Various material characterization techniques reveal that the increase in impedance is due to factors such as cracking of the anode graphite layer and localized lithium plating on the anode. Furthermore, the experiments reveal that the aluminum current collector in the short-circuit area dissolves and diffuses to the anode surface, forming deposits, while deposits also form around the impurity particles in the cathode. These phenomena can further degrade battery performance. The findings of this study enhance the understanding of the deep-seated effects of impurities in lithium-ion cells and provide theoretical insights for the manufacturing and detection methods of internal impurities in lithium-ion cells.

Keywords: lithium-ion battery, metal impurity, internal short circuit, polarization increasing, collector corrosion

NONMENCLATURE

Abbreviations	
XRM	X-ray microscopy
SEM	Scanning electron microscopy
EDS	Energy-dispersive X-ray spectroscopy
OM	Optical microscope
SOC	State of charge

1. INTRODUCTION

In recent years, lithium-ion batteries have been widely used in electric vehicles and energy storage stations due to their high energy density and long cycle life. The manufacturing processes of lithium-ion batteries demand strict environmental and procedural standards. However, during the electrode slitting and tab welding processes, metal debris and welding slag, such as copper particles, may be generated. These copper impurity particles can reside within the cell and potentially induce internal short circuit[1], which may be one of the causes of thermal runaway accidents[2].

Several studies have been conducted by researchers to address the issue of impurities within cells. Wu[3] and Qian[4] used X-ray microscopy (XRM) for in-situ observation of commercial cells, revealing the presence of impurities within certain cells. Zheng[5] studied the self-discharge of defective cells with different impurity types and impurity locations, and found that metal impurities between the cathode and the separator can cause more than 90% of the cells to exhibit self-discharge abnormalities. Kong[6] discovered that impurity particles inside the cell can induce short circuits between the aluminum current collector and the graphite anode, potentially leading to cell self-ignition. Sun[7,8] found that copper particles in lithium-ion cells dissolve at high potentials and deposit within the pores of the separator, thereby inducing internal short circuits.

Although the aforementioned studies have yielded some results, the impact of impurities on the microstructure of the battery remains incompletely understood. In this paper, impurity-containing cells and normal cells are prepared on the battery production line. Both types of cells are subjected to charge-discharge cycling. XRM is used to reveal the types of internal short circuits in the impurity-containing cells, while scanning

This is a paper for the 16th International Conference on Applied Energy (ICAE2024), Sep. 1-5, 2024, Niigata, Japan.

electron microscopy (SEM) and energy-dispersive X-ray spectroscopy (EDS) are employed to investigate the fundamental reasons for the higher polarization in impurity-containing cells compared to normal cells. These findings provide a theoretical reference for the manufacturing of lithium-ion batteries and methods for detecting internal impurities.

2. MATERIAL AND METHODS

2.1 Cell preparation

As illustrated in Fig. 1, the cell manufacturing process involves mixing, coating, pressing, slitting, stacking, casing, electrolyte injection, and sealing. Copper particles are selected under an optical microscope (OM) and then incorporated into the cell during the stacking process. The parameters of the prepared cells and the impurities are listed in Table 1.

Fig. 1 Schematic diagram of the cell manufacturing process

2.2 Charge and discharge test

After the preparation of both normal and impurity-containing cells, an initial formation process is required, followed by three charge-discharge cycles for preconditioning. Subsequently, all cells undergo 20 charge-discharge cycles under identical conditions. The experimental environment is maintained at a constant temperature of 25°C. The charging condition is constant current-constant voltage (CC-CV) mode, and the discharging condition is constant current (CC) mode, with both charging and discharging currents set at 2 A. After the cycling process is completed, the cells are left to rest at 100% state of charge (SOC) to measure the self-discharge rate, which is used to assess the presence and extent of internal short circuits. A pressure of 24.3 kPa is applied to the surface of the pouch cell during charging, discharging, and resting to simulate the pre-tension force within an actual battery pack. The charging and discharging of the cells are conducted using a charge-discharge device (CT3002K, LANHE, China), while the ambient temperature is regulated by an environmental chamber (RH/GDW-225, Ronghua, China).

2.3 Material characterization techniques

To thoroughly investigate the mechanisms by which impurities affect the microstructure of cells, nondestructive observations are first conducted using XRM(Xradia 520 Versa, Carl Zeiss, Germany). Subsequently, the impurity-containing cells are disassembled in an argon-filled glove box to separate the anode and cathode layers containing the impurities. The surface morphology of the electrode near the impurity particles is examined using OM(M125, Leica, Germany) and SEM(RISEMAGNA, Tescan, Czech Republic). Additionally, the presence and distribution of elements are analyzed in conjunction with EDS(RISEMAGNA, Tescan, Czech Republic).

Table. 1 Parameters of the cells and the impurities

	parameters	Values
Cell	Type	Pouch
	Anode material	Graphite
	Cathode material	NCM811
	Capacity	About 2.8 Ah
	Size	110 mm*55 mm*3 mm
	Anode layers	11
	Cathode layers	10
Impurity	Element	Cu
	Shape	Spherical
	Diameter	400±10 μm
	Amount	About 10
	Location	Between cathode and separator

3. RESULTS AND DISCUSSION

3.1 Voltage characteristics of impurity-containing cells

The results of cell resting at 100% SOC are illustrated in Fig. 2(a). It can be observed that during the initial stage of resting, there is minimal difference in voltage drop between the normal cells and the cells containing

impurities. This phenomenon arises from the predominant polarization of the cell during this stage. However, as time progresses, the voltage of the impurity-containing cells steadily decreases, while the voltage of the normal cells remains relatively stable. This indicates the occurrence of internal short circuits in the impurity-containing cells. From Table. 2, it is evident that the self-discharge rate coefficient (K value) of the impurity-containing cells is significantly higher than that of the normal cells.

Table. 2 Self-discharge rates of the cells

Cell index	Normal cell			Impurity-containing cell		
	#1	#2	#3	#4	#5	#6
K value （mV/h）	0.17	0.16	0.17	2.95	2.53	1.70

Additionally, the upper parts of Fig. 2b and Fig. 2c show the voltage curves during the charging process and the resting period after the cells are fully charged, respectively. In the quantitative evaluation of internal short circuits, many studies have used thermocouples implanted within the cell as a substitute experiment for internal short circuits. However, the short-circuit resistance in such methods is typically constant, which differs from the short circuits induced by impurities inside the cell under actual conditions. Therefore, a quantitative evaluation of the short-circuit degree in impurity-containing cells in different voltage ranges is conducted.

The methods for obtaining internal short-circuit resistance include not only model-based approaches, such as equivalent circuit models and electrochemical models, but also non-model-based approaches. For instance, this study applies a non-model-based method that calculates the internal short-circuit resistance based on data from fixed voltage intervals during the charging process. When an internal short circuit occurs in the battery, the short-circuit current can be obtained by dividing the voltage by the internal short-circuit resistance. By integrating this current over the time interval during which the voltage increases from u1 to u2, Eq. (1) is derived.

$$\int_{t_{u1}}^{t_{u2}} I_{isc}\,dt = \int_{t_{u1}}^{t_{u2}} \frac{U(t)}{R_{isc}}\,dt \tag{1}$$

Where I_{isc} is the internal short-circuit current, U is the voltage, t_{u1} is the time when the voltage is u_1, t_{u2} is the time when the voltage is u_2, and R_{isc} is the internal short-circuit resistance.

Assuming that the short-circuit resistance remains constant within this interval, the internal short-circuit resistance can be calculated using Eq. (2).

$$R_{isc} = \frac{\int_{t_{u1}}^{t_{u2}} U(t)dt}{\Delta Q} \tag{2}$$

Where ΔQ represents the difference in the amount of charge added to a normal battery and an internally short-circuited battery within the same charging voltage interval.

The calculated results of the short-circuit resistance are presented in Table. 3. It is evident that the internal short-circuit resistance of impurity-containing cells is significantly higher in the high SOC range compared to the low SOC range. This is attributed to the mechanical expansion of the electrode, which alters the contact area between the impurity particles that pierce the separator and the active material of anode.

Table. 3 Internal short-circuit resistance values in different voltage ranges

u_1 (V)	u_2 (V)	R_{isc1} (Ω)	R_{isc2} (Ω)	R_{isc3} (Ω)
3.6	3.8	65.96	69.24	75.25
3.8	4.0	51.05	54.14	59.98
4.0	4.2	44.32	46.89	50.81

u_1: the lower boundary voltage of calculation interval, u_2: the upper boundary voltage of calculation interval, R_{isc1}(R_{isc2}, R_{isc3}): the internal short-circuit resistance of the first (second, third) impurity-containing cell.

By averaging the voltages of three normal cells as a baseline and then subtracting the voltages of three impurity-containing cells from this baseline, the differential voltage curves are obtained, as shown in the middle sections. The lower sections depict the rate of voltage change. It can be observed that the voltage differences gradually decrease due to the presence of internal short circuits in the impurity-containing cells. Additionally, the voltage difference values in several impurity-containing cells show a peak during the initial stage of charging. This peak is influenced by the material properties, where the rate of voltage change is relatively high at this specific voltage. Consequently, a minor difference in charge between the impurity-containing cells and the normal cells during the initial stage results in a significantly larger voltage difference. Furthermore, the voltage difference values for the three impurity-containing cells are greater than zero at the beginning of charging, indicating that the polarization of the impurity-containing cells is higher than that of the normal cells. To elucidate the reasons for the differences in polarization,

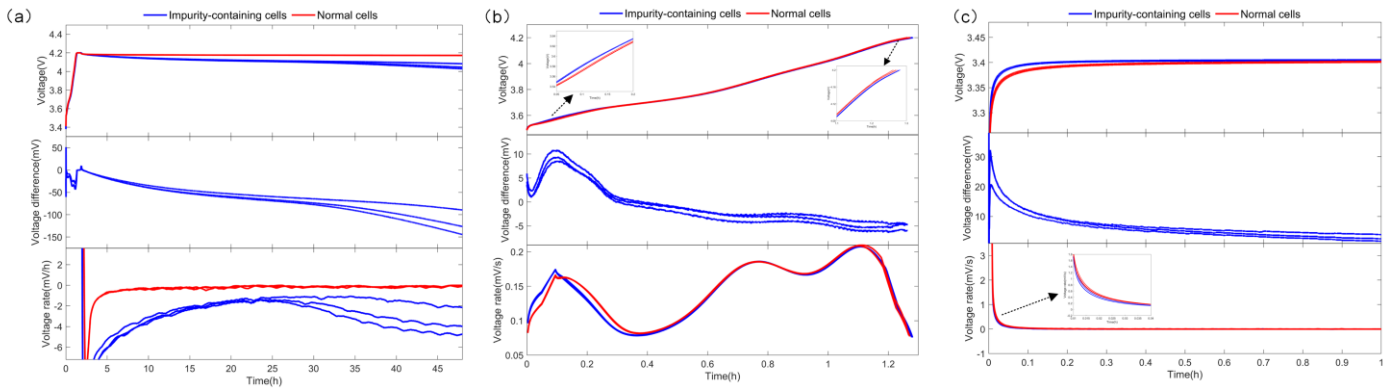

Fig. 2 Voltage, voltage difference, and voltage rate curve during: (a) resting at 100% SOC; (b) constant charging; (c) resting at 0% SOC

the types of internal short circuits, and other effects caused by impurities, nondestructive observations and microscopic structural examinations after disassembly are conducted.

3.2 Microstructural characterization of impurity-containing cells

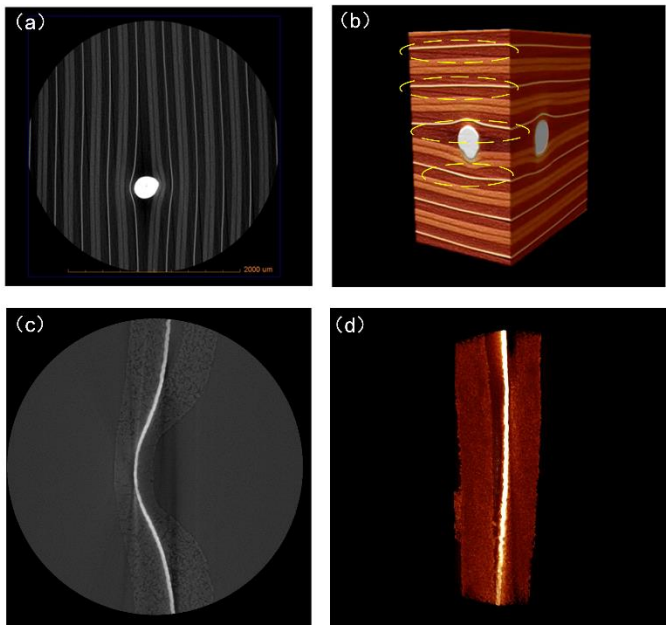

Fig. 3 Results of XRM observations: (a) cross-section image_3μm; (b) 3D reconstructed image_3μm; (c) cross-section image_0.7μm;(d)3D reconstructed image_0.7μm

First, the structure around the impurities is observed using XRM. Fig. 3a shows a cross-sectional view with a voxel resolution of 3 μm, where the impurities compress the electrode sheets, causing deformation. The 3D reconstruction in Fig. 3b provides a clearer view, revealing that the impurity particles did not completely penetrate the active materials of the cathode and anode. Therefore, the internal short circuit in this cell is between the NCM cathode and graphite anode, which is the least dangerous among the four types of short circuits[9]. However, if the impurity particles are larger, they are likely to penetrate the active materials of both the cathode and anode, potentially contacting the current collector and leading to more dangerous types of short circuits. To enhance the electrochemical performance and safety of the battery, the size of impurity particles within the cells must be strictly controlled. Additionally, the compression from the impurities has caused cracks in multiple layers of graphite, as highlighted by the yellow box in Fig. 3b. To observe the cracks more clearly, the pouch cell is scanned at a higher voxel resolution of 0.7 μm. As shown in Fig. 3c and Fig. 3d, the presence of internal impurity particles has caused partial detachment of the active material layer around these particles from the current collector, which leads to increased polarization in the impurity-containing cell.

Subsequently, the impurity-containing cells are disassembled in a glove box to obtain the specific layers of the anode and cathode where the impurities are located. SEM then used to observe the areas around the impurities. As shown in Fig. 4a, the surface of the graphite anode is indented by the Cu impurity particles. Interestingly, many small particles, approximately 500 nm in size, are found within these indentations. The magnified view in Fig. 4b clearly shows the presence and aggregation of these small square particles.

To identify these particles, elemental analysis is performed using EDS. Fig. 4c and Fig.4d reveal that these small particles within the indentations contain Al. Since Al is only present in the cathode current collector of the cell, this indicates that the cathode current collector underwent corrosion. This corrosion may have been caused by the high temperature at the short-circuit points, leading to the decomposition of the electrolyte and the formation of HF, which subsequently corroded

the current collector [10]. The Al^{3+} then diffuse to the anode surface with the electrolyte and deposited there due to the low potential. The presence of oxygen in Fig. 4e is likely due to the oxidation of Al on the anode surface to Al_2O_3 after the battery was disassembled and exposed to air.

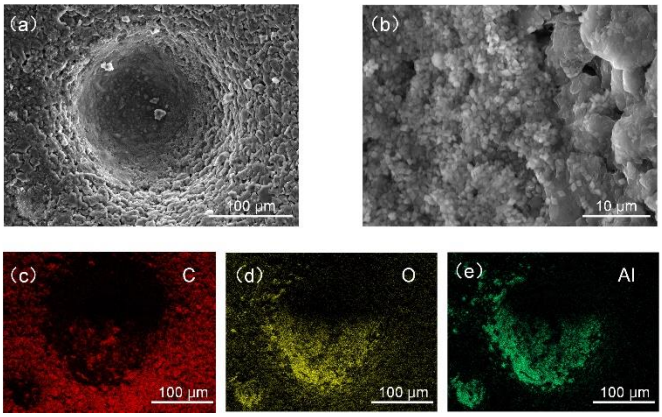

Fig. 4 Anode surface characterization of Cu particle area: (a) SEM image (1 kx); (b) SEM image (8 kx);(c) C distribution; (d) O distribution; (e) Al distribution

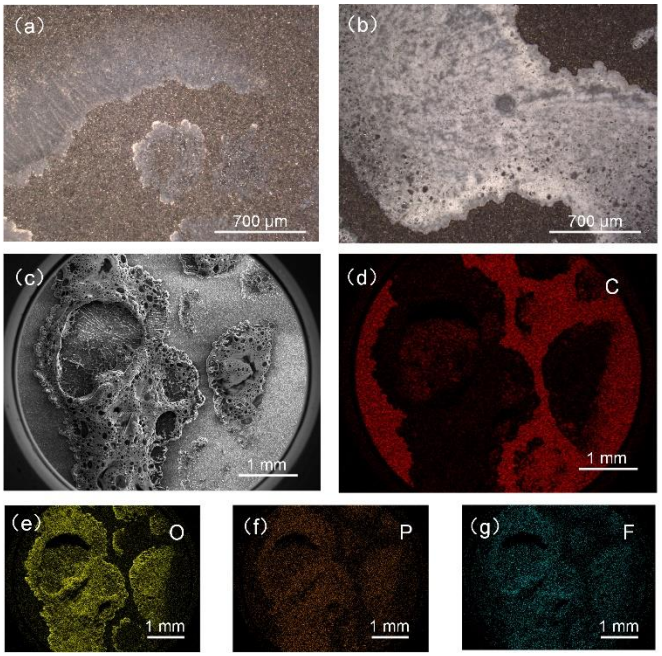

Fig. 5 Anode surface characterization of sediment area: (a) initial optical microscope image; (b) optical microscope image after 1 minute of exposure; (c) SEM image; (d) C distribution; (e) O distribution; (f) P distribution; (g) F distribution

In addition to the deposition of Al, other deposits were observed on the anode surface. As shown in the optical microscope image in Fig. 5a, these deposits reacted vigorously when exposed to air, and after approximately 1 minute, their morphology appeared as shown in Fig. 5b. The electron microscope image in Fig. 5c reveals a loose, porous structure. The EDS images in Fig. 5d, Fig. 5e, Fig. 5f and Fig. 5g indicate that these deposits mainly contain O, P, and F elements. It can be inferred that these deposits are formed from lithium plated on the anode surface, reacting with water and oxygen in the air. The lithium plating on the anode surface is associated with anode cracking, which will further contribute to increased cell polarization.

As illustrated in Figure 6a, there are deposits surrounding the impurity particles on the cathode surface. EDS analysis reveals that these deposits are primarily composed of F, P, and Cu elements, as shown in Fig. 6b, Fig. 6c, and Fig. 6d. This phenomenon is attributed to the dissolution of copper at high potentials, along with the deposition of electrolyte reaction by-products around the impurity particles.

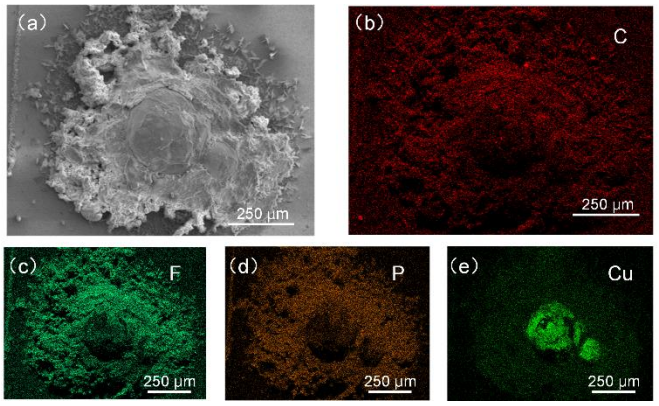

Fig. 6 Cathode surface characterization of Cu particle area: (a) SEM image; (c) F distribution; (d) P distribution; (e) Cu distribution;

4. CONCLUSIONS

This study comprehensively investigates the impact of impurity introduction on cell performance using various material characterization techniques. The results indicate that, compared to normal cells, impurity-containing cells exhibit internal short circuits induced by copper particles penetrating the separator, leading to anode-cathode shorts. Additionally, these cells experience greater polarization during charge-discharge cycles, primarily due to the cracking of graphite layers in the anode and localized lithium plating. Furthermore, the experiments reveal that the aluminum current collector in the short-circuit area dissolves and diffuses to the anode surface, forming deposits, while deposits also form around the impurity particles in the cathode. These microstructural changes will further degrade battery performance. The findings of this study enhance the understanding of the profound impacts of impurities in lithium-ion cells and provide theoretical insights for the

manufacturing and detection methods of internal impurities in lithium-ion cells.

ACKNOWLEDGEMENT

This work is funded by the National Natural Science Foundation of China (Grant No. 52177218), National Natural Science Foundation of China (Grant No. 52307244), the Natural Science Foundation of Shanghai (Grant No. 23ZR1429100) and Natural Science Foundation of Jiangsu Province (Grant No. BK20210773).

REFERENCE

[1] Grabow J, Klink J, Benger R, et al. Particle Contamination in Commercial Lithium-Ion Cells-Risk Assessment with Focus on Internal Short Circuits and Replication by Currently Discussed Trigger Methods[J]. Batteries, 2023, 9(1): 9.

[2] Hu G, Huang P, Bai Z, et al. Comprehensively analysis the failure evolution and safety evaluation of automotive lithium ion battery[J]. eTransportation, 2021, 10: 100140.

[3] Wu Y, Saxena S, Xing Y, et al. Analysis of Manufacturing-Induced Defects and Structural Deformations in Lithium-Ion Batteries Using Computed Tomography[J]. Energies, 2018, 11(4): 925.

[4] Qian G, Monaco F, Meng D, et al. The role of structural defects in commercial lithium-ion batteries[J]. Cell Reports Physical Science, 2021, 2(9): 100554.

[5] Zheng L, Wan L, Chen Z, et al. Effects of impurities on the self-discharge of Li-ion battery [J]. Battery Bimonthly, 2022, 52(4): 419-422.

[6] Kong X, Lu L, Yuan Y, et al. Foreign matter defect battery and sudden spontaneous combustion[J]. eTransportation, 2022, 12: 100170.

[7] Sun Y, Yuan Y, Lu L, et al. A comprehensive research on internal short circuits caused by copper particle contaminants on cathode in lithium-ion batteries[J]. eTransportation, 2022, 13: 100183.

[8] Sun Y, Yuan Y, Lu Y, et al. Life-cycle evolution and failure mechanisms of metal-contaminant defects in lithium-ion batteries[J]. Journal of Power Sources, 2023, 557: 232591.

[9] Liu B, Jia Y, Li J, et al. Safety issues caused by internal short circuits in lithium-ion batteries[J]. Journal of Materials Chemistry A, 2018, 6(43): 21475-21484.

[10] Gabryelczyk A, Ivanov S, Bund A, et al. Corrosion of aluminium current collector in lithium-ion batteries: A review[J]. Journal of Energy Storage, 2021, 43: 103226.